# Electric Vehicle Charging Based on Inductive Power Transfer Employing Variable Compensation Capacitance for Optimum Load Matching

Grazian, Francesca; Shi, Wenli; Soeiro, Thiago Batista; Dong, Jianning; Bauer, Pavol

**DOI**
10.1109/IECON43393.2020.9254920

**Publication date**
2020

**Document Version**
Final published version

**Published in**
IECON 2020 The 46th Annual Conference of the IEEE Industrial Electronics Society

# Electric Vehicle Charging Based on Inductive Power Transfer Employing Variable Compensation Capacitance for Optimum Load Matching

Francesca Grazian, Wenli Shi, Thiago Batista Soeiro, Jianning Dong, and Pavol Bauer
Electrical Sustainable Energy Department
Delft University of Technology, Delft 2628 CD, The Netherlands
Email: (F.Grazian, W.Shi-3, J.Dong-4, T.BatistaSoeiro, P.Bauer)@tudelft.nl

***Abstract*—In inductive power transfer applications, it is possible to ensure high efficiency of the main coils by operating at the optimum load. Since the optimum load depends on the coupling between the main coils, the operation needs to be adapted to match this case at different alignment conditions. This paper proposes a method to keep the optimum load constant by varying the natural resonant frequency of both the primary and secondary circuits of a S-S compensation network. This is possible by changing the value of the compensation capacitors at different alignments. This strategy differs from the ones found in the literature, where the input and the output voltage are changed to always match the optimum load. The proposed concept is proven through circuit simulations of an 11 kW EV battery charging system, and several strategies for the implementation of the variable capacitance are discussed.**

***Index Terms*—Electric vehicles, inductive power transfer, optimum load matching, variable capacitance, wireless charging.**

## I. Introduction

In the last decade, inductive power transfer applications have been reaching high power-transfer efficiencies when using resonant passive networks. For example, in [1], it has been measured a DC-DC peak efficiency of 96.0% at 7.7 kW output power by using rectangular coils compensated by a double-sided LCC network. Additionally, a DC-DC peak efficiency of 95.8% has been achieved in [2] at 50 kW output power with rectangular coils compensated by a series-series (S-S) network. These promising results make electric vehicle (EV) wireless charging still competitive with respect to the charging through cables, especially in some specific applications such as autonomously driven EVs, public transportation using opportunity wireless chargers and/or dynamic charging roads.

In relatively high-power applications, the resonant current that flows through the main coils might have a considerable amplitude. For instance, in [3], the sinusoidal current that flows in the S-S compensated coils of the 50 kW wireless charging system has a peak value over 100 A. Therefore, to ensure high efficiency, the system must work in the operating condition that minimizes the ohmic losses of the main coils while delivering the rated output power. As discussed in [4], it exists an equivalent resistive load for each coupling condition that minimizes those coils' losses, and it takes the name of optimum load. In other words, the efficiency of the coils is maximized when the equivalent impedance of the system matches the optimum load. However, since the coupling condition is generally not fixed in EV wireless charging, the optimum load is not fixed as well. This means that the operating point needs to be adjusted to ensure the highest coils' efficiency at different alignments. Additionally, it is important to operate the inverter slightly above the natural resonant frequency of the system such that the active semiconductors' zero voltage switching (ZVS) turn-on is ensured [1].

The control strategy based on the optimum load matching has been investigated, especially for the series-series compensation network. In [5]–[8], the optimum load is always matched by controlling the DC voltage at the receiver side through a DC/DC converter. In this way, it is possible to control the ratio between the output voltage and current such that the optimum load for that coupling condition is reached. Moreover, the output power is set to the rated value by controlling the input voltage at the transmitter side through either a DC/DC converter, a grid-connected AC/DC converter or an adjustable DC power supply. Moreover, by operating slightly above the resonant frequency, the ZVS soft-switching of the inverter is also ensured. This strategy of DC-voltage control maximizes the efficiency of the coils, but it must be taken into account that the additional power converters introduce extra losses, costs, higher components count, and above all, it most likely worsen power density. On the other hand, [9] executes both the optimum load matching and output power control by asymmetrically phase-shifting both the transmitter- and rectifier-side high-frequency converters, respectively. This system does not use additional DC/DC converters but active semiconductors for the converters at both sides. Additionally, the soft-switching of both converters is guaranteed by using variable capacitors, which sets the operation in the inductive region. By using the phase-shifting strategy, the coils' ohmic losses can be minimized at the cost of increasing the reactive power at partial load which, in turn, reduces the total efficiency. The common characteristic of these control strategies is that, once the optimum load changes due to variations in the magnetic coupling, the input and the output voltages are adjusted such that the optimum load is continuously matched. On the other hand, the value of the optimum load could be kept constant over the coupling variations by changing the natural resonant frequency of the system, which results from modifying the value of the resonant

978-1-7281-5414-5/20/$31.00 ©2020 IEEE

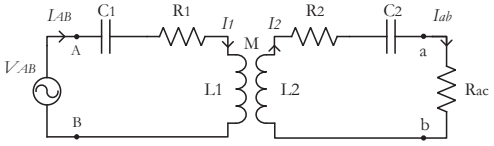


Fig. 1. Equivalent circuit of the S-S compensation network.

components.

This paper explains an optimum load matching strategy that consists of varying the natural resonant frequency of the system when the misalignment occurs. This can be achieved by adjusting the compensation capacitors' value. The S-S compensation network of an 11 kW EV battery charger is considered. The analytical modeling of the optimum load matching is explained in Section II, where different implementations are discussed. The proposed strategy that uses variable capacitors has been simulated, and the results can be found in Section III. After having verified the functionality of the proposed concept, possible implementation strategies for the variable capacitors are discussed in Section IV. Finally, conclusions are given in Sections V.

## II. Optimum load matching

The equivalent resistive optimum load $R_{ac,opt}$ that optimizes the efficiency of the main coils has been defined in [4] for all the basic compensation networks (series-series, series-parallel, parallel-series, parallel-parallel). Therefore, for the S-S compensation network in Fig. 1, the optimum load $R_{ac,opt}$ is the solution of (1) which expression is shown in (2). The latter can be approximated when $k^2Q_{1c}Q_{2c} \gg 1$ [8]. When the AC resistances $R_1$, $R_2$ are modeled as the lump equivalent series resistance of the whole circuit (power electronics, compensation capacitor and coil), $R_{ac,opt}$ maximises the efficiency of the entire wireless charging system and not only of the coils.

$$\frac{d}{dR_{ac}}\left(\frac{P_1+P_2}{P_{ac}}\right) = \frac{d}{dR_{ac}}\left(\frac{R_1I_1^2+R_2I_2^2}{R_{ac}I_{ab}^2}\right) = 0 \tag{1}$$

$$R_{ac,opt} = \sqrt{\frac{L_2}{C_2}}\frac{\sqrt{1+k^2Q_{1c}Q_{2c}}}{Q_{2c}} \cong \omega_0 k\sqrt{L_1L_2}\sqrt{\frac{R_2}{R_1}} \tag{2}$$

From (2), it can be noticed that $R_{ac,opt}$ highly depends on the magnetic coupling factor $k$. This means that, for each value of $k$, it exists an optimum load $R_{ac,opt}$. To ensure maximum efficiency of the coils, the operating load $R_{ac}$ needs to match the optimum load, i.e. the condition $R_{ac} = R_{ac,opt}$ must be satisfied. Additionally, when misalignment occurs, the delivered output power $P_{ac} = R_{ac,opt}I_{ab}^2$ must be kept constant to the rated value. As a matter of fact, the power $P_{ac}$ would vary at different values of $k$ for the same input voltage $V_{AB}$ because of the load-independent output current:

$$I_{ab} = I_2 = \frac{V_{AB}}{j\omega M} \tag{3}$$

The equivalent circuit in Fig. 1 is used generally for the analysis in the frequency domain, but it is a simplification of the actual circuit employed in EV wireless charging systems. As a matter of fact, the high-frequency input voltage $V_{AB}$ is typically created from a DC voltage supply via an H-bridge inverter. Moreover, since the output load is a battery that needs to be charged, the high frequency voltage induced at the secondary circuit must be rectified. As a consequence, it is reasonable to consider that EV wireless charging systems have a DC voltage at both the input and output. Additionally, DC/DC converters can be placed at both the input and output ports of the system, such that the power and battery's voltage requirements are met. According to the previous considerations, a more realistic circuit of an EV wireless charging system is shown in Fig. 2(a) where the DC/DC converters are included for both transmitter- and receiver-side circuits, while Fig. 2(b) shows the case without DC/DC converters.

When the H-bridge inverter is used as shown in Fig. 2, the inverted high-frequency voltage $V_{AB}$ is a square waveform that swings between $\pm V_{in}$. On the other hand, in the equivalent circuit of Fig. 1, the fundamental -or first- harmonic component of $V_{AB}$ is used for the frequency-domain analysis. Therefore, the relation between the DC input voltage $V_{in}$ and the fundamental harmonic component of $V_{AB}$ is described in (4) where $\hat{V}_{AB}$=$\sqrt{2}V_{AB}$ is the peak value, and $V_{AB}$ is the root-mean-square (RMS) value. Additionally, the total DC load of the circuit in Fig. 2(a) can be represented with the equivalent resistive load $R_L$ in Fig. 2(b). According to [10], the relation between $R_L$ and the high-frequency load $R_{ac}$ in Fig. 1 is described in (5), and the relation between the DC output current $I_{out}$ and the high-frequency output current $I_{ab}$ in (3) is shown in (6). Moreover, for $R_L = R_{L,opt}$, the DC output voltage $V_{out}$ in (7) can be computed by combining (2), (5), and (6).

$$V_{in} = \frac{\pi}{4}\hat{V}_{AB} \tag{4}$$

$$R_L = \frac{\pi^2}{8}R_{ac} \tag{5}$$

$$I_{out} = \frac{2}{\pi}\hat{I}_{ab} = \frac{2}{\pi}\frac{\frac{4}{\pi}V_{in}}{j\omega M} \tag{6}$$

$$V_{out} = \frac{\pi}{4}\hat{V}_{ab} = R_L I_{out} \tag{7}$$

Besides matching the optimum load condition, it is important to charge the battery with its rated power $P_{batt}$. In the case of high efficiency at the receiver-side DC/DC converter in Fig. 2(a), it is reasonable to assume a lossless operation ($P_{batt} = P_{out}$) as a first approximation. From (6), the computation of $P_{out}$ results in (8), where $V_{out}$ is shown in (7) for the optimum load operation.

$$P_{out} = V_{out}I_{out} = \frac{8}{\pi^2}\frac{V_{in}V_{out}}{\omega_0 k\sqrt{L_1L_2}} \tag{8}$$

At different misalignment conditions, it is possible to make sure that the operation matches the optimum load, i.e. that $R_L = R_{L,opt} = \frac{\pi^2}{8}\omega_0 k\sqrt{L_1L_2}\sqrt{\frac{R_2}{R_1}}$ by either controlling the input and output voltage levels, or by changing the natural resonant frequency of the system through variable capacitors. These two strategy are explained in the following paragraphs.

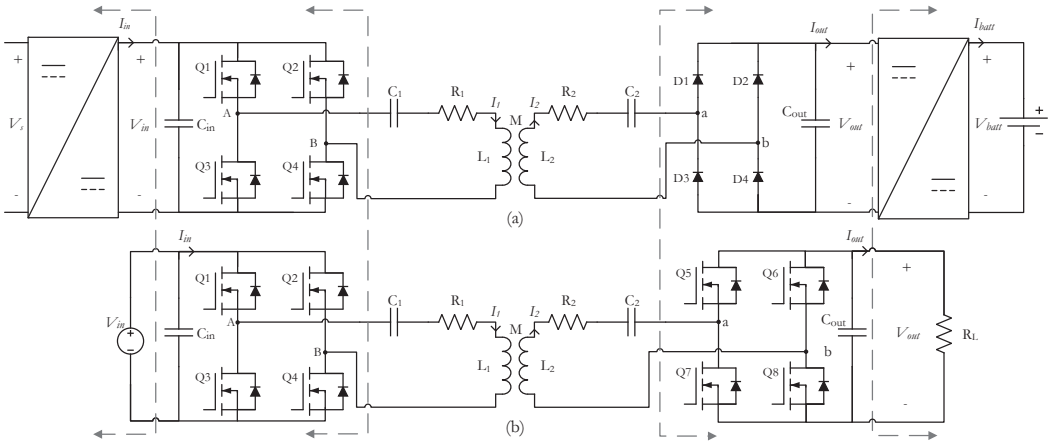


Fig. 2. Examples of complete circuit for EV wireless charging. Hereby, the optimum load matching is commonly achieved by regulating both the input and output voltages through: (a) DC/DC converters, (b) phase-shift control.

### A. Control of both the input and the output voltages

In [5], the optimum load matching is achieved by controlling both the input and output DC voltages which is possible through the circuit in Fig. 2(a). On the other hand, in [9], the optimum load matching is achieved by phase shifting both the input and output converters to control the amplitude of the fundamental harmonic component of both $V_{AB}$ and $V_{ab}$. The latter can be realized through the circuit in Fig. 2(b). Therefore, the two implementations in [5] and [9] differ in the circuit topology but they implement similar concept.

The first step of this concept is to compute the value of $R_{L,opt}$ based on the circuit parameters and the coupling condition. The optimum load can be matched by controlling the receiver-side voltage such that $V_{out}$ (or $V_{ab}$) is equal to (7), where $R_L = R_{L,opt}$. After this, $P_{out}$ must equal the rated power level of the battery. From (8), the latter can be ensured by controlling the input voltage $V_{in}$ (or $V_{AB}$) according to (9).

$$V_{in} = \frac{\pi}{4}\hat{V}_{AB} = \frac{\pi^2 \omega_0 k \sqrt{L_1 L_2} P_{out}}{8 V_{out}} \tag{9}$$

The optimum load matching through voltage control works at fixed frequency of the inverter, and it requires either the operation of the DC/DC converters or the insertion of reactive power in both the primary and secondary circuits which lower the total efficiency of the EV wireless charging system.

### B. Control of the system's natural resonant frequency

Since the optimum load is $R_{L,opt} = \frac{\pi^2}{8}\omega_0 k \sqrt{L_1 L_2}\sqrt{\frac{R_2}{R_1}}$, varying the natural resonant frequency $\omega_0$ of the compensation network could counteract the variations of $k$. Since in the actual system it might be hard to access the main coils, it is preferable to vary $\omega_0$ by changing the value of the compensation capacitors $C_1$ and $C_2$. Then, it is possible to keep $R_L = R_{L,opt}$ constant by adapting the inverter's operating frequency such that it matches the system's resonant frequency and, consequently, $P_{out}$ would be also constant.

Hereby, the total efficiency of the wireless charging systems is most likely higher than in the implementations that control the input and output voltages because there is no need of neither DC/DC converters or injecting reactive power to match different values of $R_{L,opt}$. With the proposed method, $R_{L,opt}$ is kept constant over the different values of $k$. However, it needs to be taken into account that the inverter's operating frequency range is limited in some applications. For example, in EV wireless charging, the frequency can be varied only in the range 79...90 kHz. As a consequence, in such applications, the variation of $k$ that can be covered is also limited. Additionally, in EV charging applications, each charging stage has a different power demand which means that $P_{out}$ would not be exactly constant. This is due to the gradual increase in $V_{batt}$ of lithium-ion batteries that takes place during most of the charging duration. According to (8), it is possible to meet the different power demands by controlling $V_{in}$ while keeping $R_L$=$R_{L,opt}$. Consequently, the charging process would be partially slowed down because the battery current $I_{batt}$ would not be constant. However, the power transfer efficiency would be maximized. Since the change in $V_{batt}$ is constrained in a limited range, the control of $V_{in}$ can be realized via the power factor correction (PFC) converter that needs to be employed for the grid-code compliance between the IPT system and the AC grid voltage.

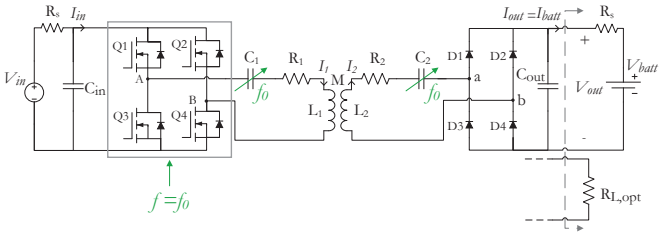


Fig. 3. Circuit used in the simulations for the operation of the constant optimum load by using variable capacitors at different alignment conditions.

## III. Proof of Concept

To prove that it is possible to achieve a constant optimum load by changing the system's resonant frequency through varying the compensation capacitors, the circuit in Fig. 3 has been simulated at different alignment conditions. The chosen system is designed for EV wireless charging

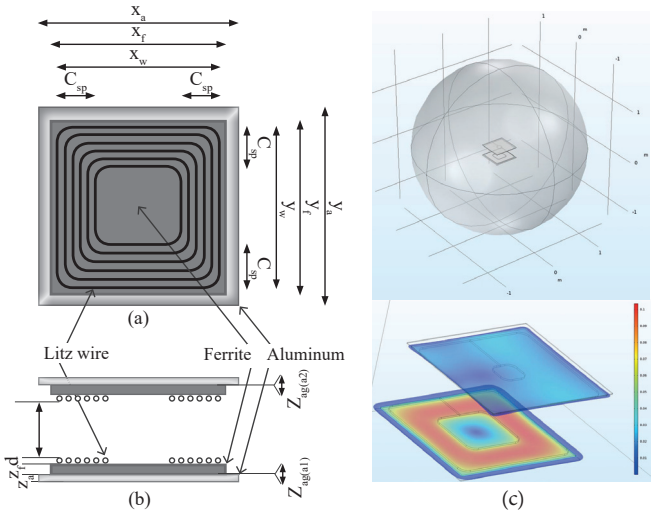


Fig. 4. Primary and secondary coils. Dimensions and geometry: (a) top view, (b) cross section. (c) Example of FEM analysis (magnetic flux density in (T)).

with the operating conditions in Table I. The inverter is composed of four SiC MOSFETs C2M0040120D, and the rectifier of eight SiC schottky diodes C4D20120H paralleled two by two. The parameters of the main coils have been selected such that the nominal operation matches the optimum load and the bifurcation phenomenon does not occur, i.e. $R_L$=$R_{L,opt}$=$\frac{V_{out}^2}{P_{out}}$ > $R_{L,bif}$, where $R_{L,bif}$ is defined in (10) for the S-S compensation network [11].

$$R_{L,bif} = \frac{\pi^2}{8}\omega_0 L_2\sqrt{1-\sqrt{(1-k)}} \tag{10}$$

The dimensions and geometry of both coils are qualitatively shown in Fig. 4(a)-(b), and they are summarized in Table II. These dimensions have been selected starting from the SAE J2954 reference design of the WPT3/Z3 VA coil [12].

Table III shows the resulting circuit parameters at both the best and the worst-allowed alignment conditions. The coils' parameters $k$, $L_1$, $L_2$ result from the finite element method (FEM) analysis performed through COMSOL Multiphysics 5.4, which an example is shown in Fig. 4(c). Moreover, $R_1$ and $R_2$ include the total series resistance of the circuit, and $C_1$, $C_2$ are the result of the specified $m$ series-connected capacitors EPCOS 6.8nF B32671L paralleled $n$ times ($m$x$n$), such that their voltage rating of $\frac{400\,\mathrm{V}}{\sqrt{2}}$ is not exceeded.

When the coils are perfectly aligned and $k$ =0.179, the compensation capacitors are tuned to resonate at the minimum allowed operating frequency of 79 kHz. The simulated circuit waveforms are shown in Fig. 5(a). Since $R_L$=$R_{L,opt}$=$\frac{\pi^2}{8}\omega_0 k\sqrt{L_1L_2}\sqrt{\frac{R_2}{R_1}}$, once the coils are misaligned, the resonant frequency of the system is increased until 90 kHz to counteract the drop of magnetic coupling such that the optimum load is kept constant. At the same time, the operating frequency of the inverter is adjusted to match the resonant frequency as shown in Fig. 5(b). In this way, the optimum efficiency of the coils can be achieved without regulating the input and output voltages. However, in EV

TABLE I
PARAMETERS OF THE CIRCUIT IN FIG. 3.

| $P_{batt}$(kW) | $V_{in}$(V) | $V_{batt}$(V) | $R_s$(Ω) | $C_{in(out)}$(μF) | $R_L$(Ω) |
|---|---|---|---|---|---|
| 10.8 | 453 | 360 | 0.5 | 60 | 12.5 |

TABLE II
DIMENSIONS (MM) OF THE MAIN COILS FROM FIG. 4.

| | $x_a, y_a, z_a$ | $x_f, y_f, z_f$ | $x_w, y_w$ | $C_{sp}$ | $Z_{ag}, Z_{ag(a)}$ | $d$ | $N$ |
|---|---|---|---|---|---|---|---|
| $L_1$ | 420, 420, 2 | 400, 400, 5 | 380, 380 | 100 | 170, 5 | 5 | 18 |
| $L_2$ | | | | 150 | | | 15 |

TABLE III
OPTIMUM LOAD MATCHING BY CHANGING $\omega_0$ OF THE EV WIRELESS CHARGING SYSTEM IN FIG. 3 WITH THE PARAMETERS IN TABLE I.

| $k$ | $L_1$(μH) | $L_2$(μH) | $R_1$(Ω) | $R_2$(Ω) | $C_1$(nF) | $C_2$(nF) |
|---|---|---|---|---|---|---|
| 0.179<br>x, y = (0, 0) cm | 205.59 | 82.42 | 0.496 | 0.381 | 19.88<br>(13x38) | 48.73<br>(6x43) |
| 0.155<br>x, y = (6.4, 0) cm<br>x, y = (0, 6.4) cm | 205.94 | 82.54 | 0.372 | 0.274 | 15.17<br>(13x29) | 37.4<br>(6x33) |

$R_1$, $R_2$ equivalent series resistance of power electronics + compensation capacitor + coil (@125°C: MOSFET $R_{ds,on}$ = 70 mΩ, diode $V_F$ = 1.4 V)

$C_1$, $C_2$ achieved by ($m$x$n$) series and parallel connections of EPCOS 6.8nF B32671L (1 kV dc, 500 V ac) ESR=80 mΩ (measured)

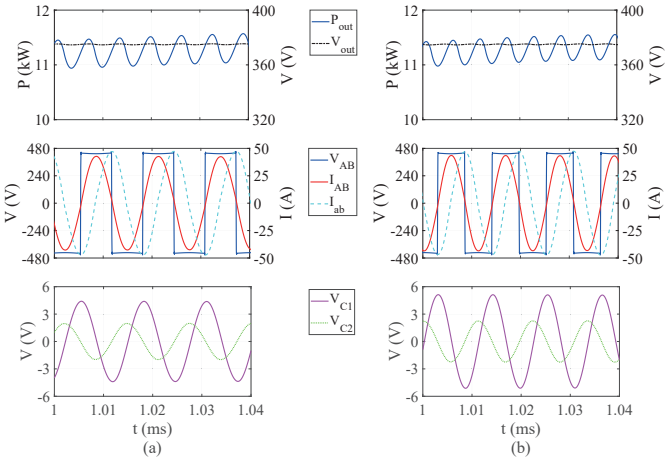


Fig. 5. Circuit simulations: (a) $k$=$k_{max}$=0.179, (b) $k$=$k_{min}$=0.155.

wireless charging, this method can cover only a limited coils' misalignment which, in this case, corresponds to a minimum coupling of $k$ =0.155 because the operating frequency has the upper limit of 90 kHz. The FEM analysis shows that the worst-allowed misalignment condition corresponds to a spacial offset of 6.4 cm in either the $x$ or $y$ direction. This spacial freedom could be enlarged further by optimizing the coils to have a lower drop of $k$ with the misalignment.

Additionally, the soft-switching of the inverter is achieved by slightly detuning the primary compensation capacitor $C_1$ such that the input impedance is inductive at the resonance.

## IV. IMPLEMENTATION OF VARIABLE CAPACITORS

The proposed method uses variable compensation capacitors to keep the optimum load constant at different coils' alignments. In this way, it is possible to eliminate the voltage control that would lower the total efficiency of the system. However, the implementation of variable capacitors can become critical in high-power wireless charging, since the capacitor voltage and current might have a high amplitude and a relatively high frequency. As an example, in the designed

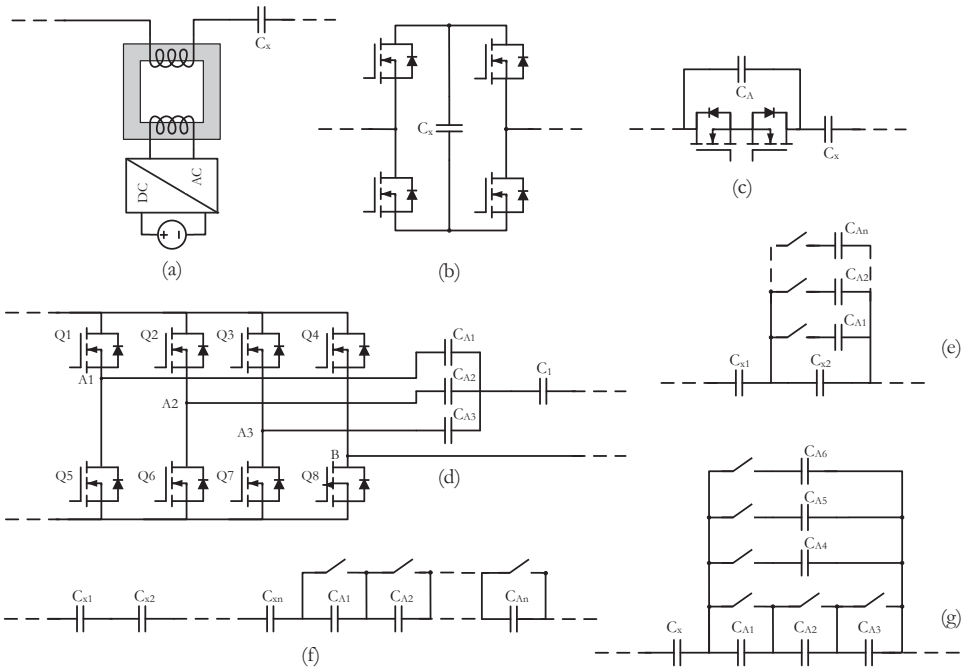


Fig. 6. Possible implementations of variable capacitors. Continuous capacitance change: (a) concept derived from the VAR compensator, (b) variation of the equivalent inductance through field cancelling, and (c) switch-controlled capacitor (SCC) [4]. Capacitance that changes in steps. Variation: (d) during the power transfer, (e)-(g) during the power transfer if semiconductor switches are used, or while there is no-power transfer if mechanical switches are used.

$11\,\mathrm{kW}$ S-S compensation network, the peak voltage across $C_1$ reaches $5.1\,\mathrm{kV}$ at the minimum coupling, with a peak current that is about $30\,\mathrm{A}$. Because of this high voltage and current stress on the compensation capacitors, suitable circuit implementation strategies need to be investigated.

Variable capacitors can have two different types of change rate: continuous change or change in steps. With the continuous change, the capacitance is changed constantly and can assume any value. For example, this can be achieved by inserting an inductor winded on a magnetic core in series to the capacitor as shown in Fig. 6(a), such that the total impedance would be $(j\omega L + \frac{1}{j\omega C})$. Around the same magnetic core, a second winding could be inserted that generates an opposing magnetic field. By controlling the current flowing through the auxiliary winding, the main magnetic field can be either partially or totally canceled. This will result in a different equivalent inductance and, consequently, in a different total impedance. This will only work if the operating frequency of the power transfer is fixed which is not the case in this application. Another concept analyzed consists of the circuit in Fig. 6(b) that resembles the static VAR compensator used in power grids. However, this is not a practical solution for high-power wireless power transfer because it would make the operation always being in a transient state. Moreover, the resulting current would be distorted, which is not acceptable because the radiated field would also be distorted. Additionally, the operating frequency used to modulate the capacitance needs to be much higher than $\omega_0$, e.g. ten times higher than $\omega_0$. This means that the modulation switches would work in hard switching conditions which is not preferable Another possible concept could be the switch-controlled capacitor (SCC) in Fig. 6(c) used in [9] for a $100\,\mathrm{W}$ wireless charging system. However, this implementation might become critical in high-power applications due to the high blocking voltage required from the solid-state switches. On the other hand, when the capacitance is changed in discrete steps, it can assume only specific values. It is preferable to have a high number of steps such that the capacitance can be set as close as possible to the target value, and, in this way, it would change almost continuously. On the other hand, a high number of steps causes a high complexity in terms of cost, size and control. Possible implementations of variable capacitors that change in steps are shown in Figure 6(d)-(g). Moreover, the compensation capacitors can be varied either during the power transfer or when no-power is transferred. Since the operating frequency is around $85\,\mathrm{kHz}$ (the period is about $11\,\mu\mathrm{s}$), solid-state based switches need to be used such that the capacitance can be changed during the power transfer. Mechanical switches cannot be used, because their typical switching time is in the order of $10\,\mathrm{ms}$. On the other hand, it is easier to change the capacitors' value when no-power is transferred which is suitable for the static wireless charging of EVs. Considering that the EV is going to be parked for a long time, the interruption of the power transfer for a few seconds have a negligible impact on the charging duration. Besides, it allows reaching a higher efficiency at a given misalignment condition, which shortens the total charging duration.

### *A. Example on the 11kW EV wireless charging system*

By taking as an example the system in Section III, the three implementations in Fig. 6(d)-(f) are compared in terms of the required number of switch units, peak voltage stress, and the

TABLE IV
DESIGN OF $C_1$ BASED ON FIG. 6.

| Fig. 6(d) | | | Fig. 6(e) | | | Fig. 6(f) | | |
|---|---|---|---|---|---|---|---|---|
| | (nF) | $mxn$ | | (nF) | $mxn$ | | (nF) | $mxn$ |
| $C_x$ | 24 | 10x35 | $C_{x1}$ | 40 | 6x35 | $C_{x1}$ | 120 | 2x35 |
| $C_{A1}$ | 40 | 5x29 | $C_{x2}$ | 8 | 8x9 | $C_{x2}$ | 120 | 2x35 |
| $C_{A2}$ | 40 | 5x29 | $C_{x3}$ | 8 | 8x9 | $C_{x3}$ | 120 | 2x35 |
| $C_{A3}$ | 40 | 5x29 | $C_{x4}$ | 8 | 8x9 | $C_{x4}$ | 120 | 2x35 |
| 6.8nF B32671L n. | | 785 | $C_{A1}$ | 8 | 8x9 | $C_{x5}$ | 120 | 2x35 |
| | | | $C_{A2}$ | 8 | 8x9 | $C_{x6}$ | 120 | 2x35 |
| | | | 6.8nF B32671L n. | | 570 | $C_{A1}$ | 120 | 2x35 |
| | | | | | | $C_{A2}$ | 120 | 2x35 |
| | | | | | | 6.8nF B32671L n. | | 560 |

total capacitors count. The primary compensation capacitor $C_1$ is taken under analysis because, as shown in Fig. 5, its voltage stress is more critical than the one of $C_2$. According to Table III, it is considered that $C_1$ ranges between 15-20 nF where the peak voltage stress varies, respectively, between 5.1-4.4 kV.

Table IV shows capacitors used for the implementations in Fig. 6(d)-(f). In particular, the values of the single capacitors are specified together with the used combination of series and parallel ($mxn$) connections of EPCOS 6.8nF B32671L capacitors that ensure a voltage stress below the rated value. Additionally, the total required number of those capacitors is shown for each implementation. As a design general rule, only identical parallel connections are allowed to make sure that the current is shared evenly. In this way, the losses are equal in the parallel branches. Additionally, to perform a fair comparison, all the implementations have been designed such that the variable capacitor can assume three values of capacitance. It need to be taken into account that more values could be achieved with the cost of increasing the circuit's complexity and cost.

Fig. 7 shows the comparison between the three implementations. The implementation in Fig. 6(f) emerges in being the most suitable because it has the least single capacitor count, it uses only 2 switch units, and it has a voltage peak stress of 690 V on the switch units that allows the use of both semiconductor and PCB-mounted high-current mechanical switches. The resulting equivalent series resistance (ESR) of the capacitors is also another important term of comparison, because it needs to be minimized to reach high efficiencies. However, it is not used here because it results in being the same for all the implementations (around 36 mΩ).

## V. CONCLUSION AND FUTURE WORK

This paper explains the concept of variable compensation capacitors employed in a S-S compensation for inductive power transfer systems to achieve a constant optimum load condition at the target output power in the presence of coils' misalignment. The functionality of this concept has been proven through circuit simulations and finite element modeling. Moreover, different implementations for the variable capacitors have been analyzed and compared. The proposed solution has higher total efficiency than traditional techniques because it do not implement neither DC/DC converters nor the injection of reactive power. However, if this concept is used in applications with limited operating frequency range such as the wireless charging of EVs, the misalignment coverage would also be limited. For this reason, this concept seems

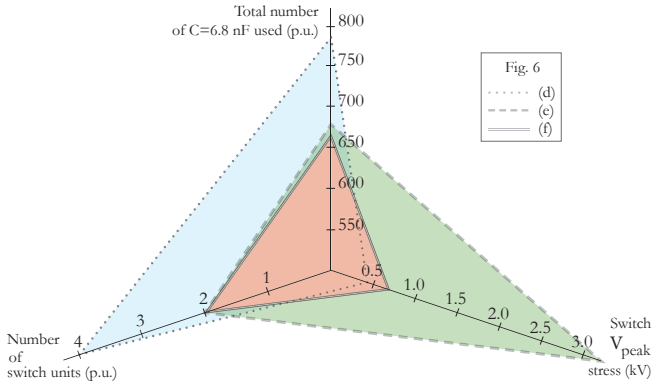


Fig. 7. Comparison of the three implementations in Fig. 6(d)-(f) in terms of switch units count, their peak voltage stress, and the total capacitor count.

to be more suitable for the static wireless charging of EVs, because, in that case, the freedom in misalignment is already limited. On the other hand, that is not the case in the dynamic on-road charging of EVs characterized by severe misalignment conditions. For these reasons, it is preferable to implement the proposed concept with coils with great misalignment tolerance. Moreover, this concept is promising for application with relatively low power because the moderated voltage and current stress on the capacitors would facilitate the implementation.

## REFERENCES


[1] S. Li, W. Li, J. Deng, T. D. Nguyen, and C. C. Mi, "A double-sided lcc compensation network and its tuning method for wireless power transfer," *IEEE Transactions on Vehicular Technology*, vol. 64, no. 6, pp. 2261–2273, 2015.

[2] R. Bosshard, U. Iruretagoyena, and J. W. Kolar, "Comprehensive evaluation of rectangular and double-d coil geometry for 50 kw/85 khz ipt system," *IEEE Journal of Emerging and Selected Topics in Power Electronics*, vol. 4, no. 4, pp. 1406–1415, 2016.

[3] R. Bosshard and J. W. Kolar, "All-sic 9.5 kw/dm3 on-board power electronics for 50 kw/85 khz automotive ipt system," *IEEE Journal of Emerging and Selected Topics in Power Electronics*, vol. 5, no. 1, pp. 419–431, 2017.

[4] W. Zhang and C. C. Mi, "Compensation topologies of high-power wireless power transfer systems," *IEEE Transactions on Vehicular Technology*, vol. 65, no. 6, pp. 4768–4778, 2016.

[5] R. Bosshard, J. W. Kolar, and B. Wunsch, "Control method for inductive power transfer with high partial-load efficiency and resonance tracking," in *International Power Electronics Conference (IPEC-Hiroshima - ECCE ASIA)*, 2014.

[6] W. X. Zhong and S. Y. R. Hui, "Maximum energy efficiency tracking for wireless power transfer systems," *IEEE Transactions on Power Electronics*, vol. 30, no. 7, pp. 4025–4034, 2015.

[7] H. Li, J. Li, K. Wang, W. Chen, and X. Yang, "A maximum efficiency point tracking control scheme for wireless power transfer systems using magnetic resonant coupling," *IEEE Transactions on Power Electronics*, vol. 30, no. 7, pp. 3998–4008, 2015.

[8] X. Tang, J. Zeng, K. P. Pun, S. Mai, C. Zhang, and Z. Wang, "Low-cost maximum efficiency tracking method for wireless power transfer systems," *IEEE Transactions on Power Electronics*, vol. 33, no. 6, pp. 5317–5329, 2018.

[9] J. Zhang, J. Zhao, Y. Zhang, and F. Deng, "A wireless power transfer system with dual switch-controlled capacitors for efficiency optimization," *IEEE Transactions on Power Electronics*, 2020.

[10] R. Steigerwald, "A comparison of half-bridge resonant converter topologies," *IEEE Transactions on Power Electronics*, 1988.

[11] S. Chopra and P. Bauer, "Analysis and design considerations for a contactless power transfer system," in *IEEE 33rd International Telecommunications Energy Conference (INTELEC)*, 2011.

[12] *J2954 RP: Wireless Power Transfer for Light-Duty Plug-In/ Electric Vehicles and Alignment Methodology*, SAE International Std., Apr. 2019.